Evaporation of nanofluid droplets with applied DC potential

Journal of Colloid and Interface Science 407 (2013) 29–38

Contents lists available at SciVerse ScienceDirect

Journal of Colloid and Interface Science

www.elsevier.com/locate/jcis

Evaporation of nanofluid droplets with applied DC potential

Daniel Orejon [a], Khellil Sefiane [a,*], Martin E.R. Shanahan [b,c,d]

[a] Institute for Materials and Processes, School of Engineering, The University of Edinburgh, King's Building's, Mayfield Road, Edinburgh EH9 3JL, United Kingdom
[b] Univ. Bordeaux, I2M, UMR 5295, F-33400 Talence, France
[c] CNRS, I2M, UMR 5295, F-33400 Talence, France
[d] Arts et Metiers ParisTech, I2M, UMR 5295, F-33400 Talence, France

ARTICLE INFO

Article history:
Received 25 January 2013
Accepted 31 May 2013
Available online 13 June 2013

Keywords:
Electrophoresis
Electrowetting
Nanofluids
Particle deposition
"Stick-slip" suppression

ABSTRACT

A considerable growth of interest in electrowetting (EW) has stemmed from the potential exploitation of this technique in numerous industrial and biological applications, such as microfluidics, lab-on-a-chip, electronic paper, and bioanalytical techniques. The application of EW to droplets of liquids containing nanoparticles (nanofluids) is a new area of interest. Understanding the effects of electrowetting at the fundamental level and being able to manipulate deposits from nanofluid droplets represents huge potential. In this work, we study the complete evaporation of nanofluid droplets under DC conditions. Different evolutions of contact angle and contact radius, as well as deposit patterns, are revealed. When a DC potential is applied, continuous and smoother receding of the contact line during the drying out of TiO_2 nanofluids and more uniform patterning of the deposit are observed, in contrast to the typical "stick-slip" behavior and rings stains. Furthermore, the mechanisms for nanoparticle interactions with the applied DC potential differ from those proposed for the EW of droplets under AC conditions. The more uniform patterns of particle deposits resulting from DC potential are a consequence of a shorter timescale for electrophoretic mobility than advection transport driven by evaporation.

1. Introduction

Due to recent advances in miniaturization, optics, electronic devices, microfluidics, and biological practices, the necessity to understand the forces and mechanisms that govern processes at smaller scales has become clear [1–3]. The production of different nanoscale particulates has also led to a new type of fluids, called nanofluids, that when added to a base fluid makes a stable suspension of modified properties, e.g., enhancing thermal conductivity or changing the dynamics of wetting, amongst others [4–6]. Therefore, interest in the problem of how these particles behave in the bulk of the fluid and how they organize at the contact line during evaporation, as well as the interactions of these fluids with the substrate and the deposits formed after the complete evaporation, has motivated many recent studies [7–12]. Although nanofluids have been studied for more than a decade now, the interplay between the phases, particles–fluid, fluid–solid, and solid–particles, is not yet fully appreciated. Recent processes and novel fluidic devices require the manipulation of small volumes of fluids, hence understanding the interfacial forces at the nanometer/micrometer scale becomes increasingly important. Previous efforts have been made to evaluate and model these interactions without an applied voltage. Following on from this, experimental work has been undertaken to try to uncover the interfacial phenomena occurring when an external electric field is applied to a droplet containing nanoparticles in suspension.

Another phenomenon that has also seen great development and increased attention within the past years is electrowetting (EW). A voltage applied to a liquid droplet prompts change in droplet shape; both contact angle and base diameter are modified from the equilibrium values. This is proposed as an active microfluidic technique capable of modifying, controlling and even moving liquid droplets with an applied voltage [1,13]. The recent interest in EW emerged due to the wide range of applications where it can be exploited. This includes the capability of manipulating small volumes of liquids and processes involving thousands of actuation cycles without any degradation [13]. Recent fields where EW has been applied include electro-optic applications, patterning, microfluidic devices for droplet mixing, lab-on-a-chip, electronic paper, more efficient electronic displays and harvesting energy from mechanical sources [14–22].

The correlation between liquid behavior and applied voltage was first observed at the end of the XIXth century by Gabriel Lippmann, who reported the dependence between electrical potential difference and change in position of a water–mercury interface

* Corresponding author at: Institute for Materials and Processes, School of Engineering, The University of Edinburgh, King's Building's, Mayfield Road, Edinburgh EH9 3JL, United Kingdom.
E-mail address: k.sefiane@ed.ac.uk (K. Sefiane).

0021-9797/$ - see front matter © 2013 Elsevier Inc. All rights reserved.
http://dx.doi.org/10.1016/j.jcis.2013.05.079

inside a capillary tube. It was found that $\partial\gamma/\partial\varphi = -q$, where q is the surface charge density, γ is the water–mercury interfacial tension, and φ is the electric potential or voltage, henceforth referred to as V [23]. The equilibrium contact angle of a droplet, small enough for gravity effects to be neglected, can be defined by Young's equation ($\gamma_{sg} - \gamma_{sl} = \gamma_{lg}\cos\theta_0$) [24] where γ_{sg}, γ_{sl} and γ_{lg} are the surface/interfacial tensions solid–gas, solid–liquid, and liquid–gas, respectively, and θ_0 the equilibrium contact angle. Combining both relationships, the well-known Young–Lippmann equation for droplets can be derived:

$$\cos\theta(V) = \cos\theta_0 + \frac{1}{2}\frac{\varepsilon_0\varepsilon_r V^2}{\gamma_{lg} d} \quad (1)$$

The change in contact angle, $\theta(V)$, is described in terms of the equilibrium contact angle, and the dielectric properties of the system, ε_r and ε_0 being the permittivity of the material and of free space, respectively, and d, the thickness of the insulating film.

Eq. (1) is valid for contact angles higher than the saturation value, which is characterized by no further observable change in θ when the voltage is increased [18,25–27]. The accepted physical mechanism for EW is that the difference in electric potential created across the droplet interface affects the solid–liquid tension, lowering the contact angle and thus increasing the base diameter. This is due to induced electric fields along the droplet surface and, in particular, in the vicinity of the triple line, modifying the equilibrium droplet shape, or even moving the whole droplet, if the gradient is high enough [28–31].

Research has been carried out to investigate the mechanisms involved when a difference of voltage is applied to a droplet. Ko et al. succeeded in visualizing internal flows within the droplet due to EW, using polystyrene particles in the microrange under AC EW conditions for different frequencies [28]. Garcia-Sanchez et al. proposed and demonstrated an increase in temperature inside the droplet as the cause of the internal flows generated at different AC frequencies to explain the hydrodynamic flows observed previously by Ko et al. [32]. The increase in temperature inside the liquid creates temperature differences along the droplet, generating both permittivity and conductivity gradients that promote internal flow at low and high AC frequencies, i.e., electrothermal effects. Mugele et al. proposed AC as a mechanism for internal droplet mixing due to capillary waves created inside the droplet [33].

Different EW techniques have led to diverse ways for studying interactions between fluid–current, colloidal suspensions–current, dielectric materials–fluid, etc. The application of an AC external voltage to a droplet modifies the bulk of the droplet, inducing hydrodynamic and electrothermal flows, as previously mentioned. On the other hand, when studying DC applied to particles in solution, the electrokinetic mechanisms present are different. Typically, oxide particles/cells/proteins/bacteria acquire surface charge when suspended in a polar liquid and, depending on this charge, the particle–particle and particle–medium interactions differ. Hence, uncovering the mechanisms that govern these interactions is of paramount importance in biological, chemical, and nanotechnological applications [34–36]. In the case of TiO_2 particles, the amphoteric nature favors the reaction of the oxide with either a hydron (H^+) or a hydroxide (OH^-) depending on the pH of the solution. When an external DC voltage is applied to these particles/cells/bacteria/proteins in suspension, there is an induced electrokinetic motion that drives these charged particles toward the electrode with opposite charge. This phenomenon is called electrophoresis (EP), studied for more than two centuries to explain how particles and ions suspended/dispersed in a fluid behave under the effect of an electric field [37]. In some cases, EP has been used as a deposition method (electrophoretic deposition, EPD) or to separate proteins or particles by size or charge [38]. Other authors using EPD succeeded in separating different TiO_2 nanoparticle sizes by controlling the time of the experiment and length of the column [39–41]. TiO_2 is commonly used in cells/bacteria studies due to the similarities in surface charge of these oxide particles with bacteria [42].

Electrowetting on dielectrics (EWOD) came to light more than two decades ago to open a new concept of EW systems aiming to obtain the same wetting effect under smaller applied electric potentials, with consequent savings in energy consumption [30,43]. Normally, EWOD systems are formed by a conductive electrode, an insulating layer, and an amorphous fluoropolymer (aFP) to separate the liquid droplet from the electric components, as explained below in Section 2. Although EWOD has been under intensive study in the past decades, little work has been dedicated to exploring EW applied to nanofluids. The experimental work of Dash et al. demonstrated the behavior of nanofluids under EWOD conditions. Bismuth telluride (Bi_2Te_3) nanoparticles of 3 nm capped with thioglycolic acid (TGA) were prepared by a microemulsion method and tested under DC conditions [44]. Greater stability and no saturation of the contact angle within the range of voltage tested due, according to the authors, to dissociation of the TGA and the nanoparticles enhancing the charge transport inside the droplet was reported.

Considering volatile droplets, since the work of Deegan et al., it has been widely accepted that the addition of nanoparticles to a base fluid promotes "stick-slip" and leads to coffee ring stain deposits [9,12,45]. During droplet evaporation, the concentration of nanoparticles in the bulk of the droplet increases with time, leading to a non-stationary process. Depending on the surface and the concentration of nanoparticles, it can result in complete pinning of the droplet, "stick-slip" or continuous receding of the contact line [9,12]. On the other hand, only few studies on the evaporation of nanofluid droplets under EW conditions have been reported paying special attention to the deposits left. In the work of Eral et al., colloidal suspensions containing 0.1 and 5 μm polystyrene particles were observed during the entire evaporation process [46]. The authors reported suppression of the coffee stain, explaining it in terms of internal flows generated within a droplet due to high AC frequencies. In a more recent publication, the suppression of this phenomenon was induced due to the oscillating movement of the contact line distinctive of AC voltages; contact line was not completely pinned, and therefore, particles did not deposit at the contact line [47]. Although AC EW seems to suppress the coffee stain, it has been demonstrated that decreasing particle size below a certain limit can lead to coffee ring formation independently of concentration or AC voltage applied [48].

Comparing AC and DC EW, it can be appreciated that the mechanisms that rule both evaporative behavior and resulting deposits during and after the complete evaporation of TiO_2 nanofluid droplets on DC EWOD systems are completely different from hydrothermal flows, capillary flows, or oscillatory movement of the CL due to the sinusoidal AC voltages applied during evaporation. Therefore, an alternative mechanism that governs the motion of TiO_2 nanoparticles suspended in a droplet under DC conditions is proposed. Although EWOD is under wide research and investigation, many aspects are still poorly understood, such as the dynamics of the CL, repulsive charges in the bulk of the droplet, internal mixing flow, and the surface tension gradient at the vicinity of the CL.

The aim of this study is to explore the effect of DC EW on deposition as the underlying mechanism to create more homogeneous deposit patterns. The interactions between fluids and EW have not been fully investigated; consequently, in this paper, we aim to contribute to understanding the different and complex mechanisms that govern both the dynamics of the contact line and the internal flow when a voltage difference is applied. The combination

of different analysis techniques and experimental methods can help to pave the way to discovering the different interactions that take place at the microscale and nanoscale.

2. Experimental

The dielectric substrate used in this study was fabricated by the Scottish Microelectronic Centre (SMC). Silicon oxide (SiO_2) was thermally grown on a silicon (Si) substrate to obtain a controlled oxide layer, and then, a 500 nm Tantalum (Ta) layer was deposited by sputtering onto the SiO_2. Thereafter, an anodizing gel was placed on top of the sputtered wafer (on the Ta), and a voltage was applied creating a uniform layer of Ta_2O_5 of thickness 95 nm. This thickness of the Ta_2O_5 layer can be controlled using different anodization voltages [30]. The last part in the fabrication process involved coating of the samples (onto the Ta_2O_5 layer) using an amorphous fluoropolymer (aFP), in this case Cytop (perfluorinated polymer consisting of C–C, C–F, and C–O bonds). It was demonstrated that using aFP as the coating for EWOD systems allows good reversibility and confers both the hydrophobicity and the insulation required [49]. The thickness of the aFP was controlled by varying the concentration of the solution and the speed during spin coating to obtain a 22 nm Cytop layer, $CYTOP_{22}$, over the Ta_2O_5. Substrates were ultrasonicated in isopropanol for 15 min and dried with a stream of nitrogen to remove any contaminant prior to the deposition of a droplet.

The properties which should be favored when fabricating these substrates can be summarized as follows: high dielectric strength to avoid breakdown of the surface when high voltages are applied, high dielectric constant, ε_r, requiring lower voltages, and a smooth and hydrophobic fluoropolymer layer in order to reduce effects of surface roughness (mechanisms of wetting).

When choosing the nanofluids, our study was motivated by many applications where TiO_2 nanoparticles can be implemented, such as pigments, in photocatalysis, in biologic applications and patterning. TiO_2 nanoparticles were purchased in powder form from Sigma Aldrich with a typical size of 25 nm; transmission electronic microscopy (TEM) was used to confirm this. Different quantities of TiO_2 were weighed and added to deionized water (two-step method) to create the following concentrations: 0.1%, 0.05%, 0.025%, and 0.01% by weight. Deionized water used for the two-step method, produced in a Barnstead NANOpure® Diamond™ Analytical ultrapure water system, had a conductivity of $18.2 \times 10^6\ \Omega$/cm, and no surfactants, salts, or additional ions were added to the system.

Solutions were ultrasonicated for several hours until no agglomerations or clusters were observed. Before deposition of the fluids onto the substrate, and previously to electrophoretic mobility (μ_{ep}) measurements, nanofluids were ultrasonicated for a further hour. Droplets of ca. 3 μl were deposited using a controlled dosing system integrated in a DSA100, Drop Shape Analyser from Krüss (Krüss GmbH, Hamburgh, Germany). This apparatus was equipped with a CCD (charge-couple device) camera (up to 25 fps, although the frame rate was adjusted to 1/8), a digitalized board (frame grabber) to connect the hardware to the computer and digitize the recorded images, a moveable sample table, and a back light to illuminate and create a contrast between the droplet, the substrate, and the surroundings. After deposition of the droplet on the dielectric substrate, a copper electrode of 91 μm in diameter connected to a DC power supply (D100 1) was inserted in the droplet. Then, voltage was increased from 0 to 18 V and thereafter kept constant at 18 V during the complete dry out.

In the case of free evaporation, the same procedure was followed; first with deposition of the droplet on the substrate, then immersion of the electrode in the droplet, followed by complete evaporation of the droplet. The recorded sequence, from droplet deposition onwards, was analyzed, and the profile properties of the droplet extracted: contact angle, θ, base radius, R, volume, V, and height, h, as a function of time. Experiments were carried out under controlled conditions: air at atmospheric pressure, 22 °C and in 30% relative humidity (RH).

Fig. 1 shows the experimental setup of EW on dielectrics. A schematic representation of charge distribution between the tantalum/tantalum pentoxide and the liquid is shown, and the dielectric layer reproducing the electric double layer formed at the solid–liquid interface [43].

Additional measurements of μ_{ep} for 0.1%, 0.05%, and 0.01% TiO_2–water were obtained using a ZetaPALS Zeta Potential Analyzer from Brookhaven Instruments Corporation and the software ZetaPALS from the same manufacturer. Approximately 1.5 mL of the nanofluid was placed in a cuvette, followed by the immersion of two parallel electrodes in this latter. Both cuvette and electrode were placed in the ZetaPALS for the measurement of the different mobilities under an applied electric field, E, varying between 6 and 9 V/cm. The zeta-potential, ζ, of the nanoparticles suspended was calculated by the same software using the Hückel equation. ZetaPALS uses Phase Analysis Light Scattering (PALS) as the method for calculation of the μ_{ep}, with a sensitivity superior to typical laser Doppler methods [50]. For each concentration, a total of 20 different measurements were averaged, and standard deviations were calculated.

Additional measurements of pH using a Laboratory pH-meter PP-15 from Sartorius and conductivity of the suspensions using the ZetaPALS Analyzer are included in Table 1. The point of zero

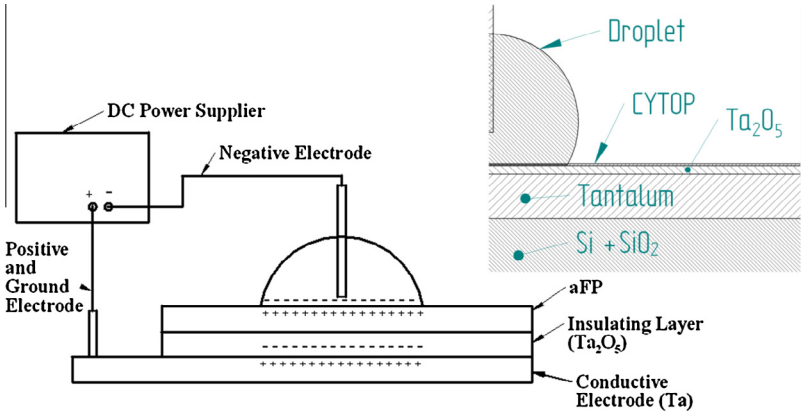

Fig. 1. Cross-sectional view of typical experimental EWOD setup. In inset: dielectric substrate, droplet, and positive/negative electrodes.

Table 1
pH and conductivity (μS), for 0.01%, 0.05%, and 0.1% of TiO_2 nanoparticle concentration by weight in deionized water.

Concentration	0.01%	0.05%	0.1%
pH	6.6 ± 0.1	6.5 ± 0.1	6.5 ± 0.1
Conductivity (μs)	87 ± 10	135 ± 15	260 ± 30

charge for these nanoparticles was found by Bhardwaj et al. for a pH ~ 5.4 [10].

3. Results

The aim of this investigation is to elucidate the underlying mechanisms involved in and during EW of TiO_2–water nanofluid droplets at different concentrations and to compare results with those of free evaporation and base fluid. Analysis of the evaporative behavior of nanofluid droplets to complete disappearance by drying out whilst subjected to an electrical voltage is presented following a basic approach where both droplet profiles and nanoparticles deposits are examined.

Prior to experiments on evaporation, work describing the EW behavior of the nanofluids for different voltages applied on the dielectric substrate $CYTOP_{22}$ was carried out. To illustrate the obtained results, the EW contact angle, θ_{EW}, versus voltage, V, applied to a 0.01% TiO_2–water nanofluid droplet is presented, in Fig. 2.

A good agreement between the experimental results and the modified Young–Lippmann theory for water is presented for voltages smaller than the saturation voltage as shown in Fig. 2, see Li et al. [30]. This latter is consistent for the different concentrations tested although results are not presented for brevity. All experiments regarding the complete evaporation and dry out of the droplet to be presented subsequently were carried out at constant voltage equal to 18 V.

In the following, the results concerning the complete evaporation of TiO_2–water nanofluids under EW conditions are presented. It is known that the addition of nanoparticles to a base fluid modifies the evaporative behavior [45] of the droplet on hydrophobic substrates, prompting the pinning of the contact line [7,9,12]. TiO_2 nanoparticles tend to cause "stick-slip" behavior of the contact line, which results in the deposition of more or less concentric rings following dry out [9]. In order to rule out any change in the evaporative behavior caused by immersion of the electrode, tests were conducted (although not included in the present paper for brevity). The results of these tests showed that, although the number of contact line jumps decreased, there was still a small, but noticeable, "stick-slip" of the contact line during free evaporation of the nanofluids tested.

Fig. 3 show the evaporative behavior of suspensions of 0.1%, 0.05%, 0.025%, and 0.01% of TiO_2 nanoparticles, under EW and no EW conditions (but with an electrode immersed to conserve basic experimental conditions). The figure shows the evolution of contact radius, R (mm), droplet height, h_0 (mm), contact angle, θ (°), versus time, t (s), and images of the deposits after complete evaporation.

When a voltage is applied to the droplet, there is a rapid increase in contact radius and a reduction in both contact angle and height, h_0. As evaporation proceeds, the shape of the droplet evolves. The contact line recedes monotonically with the absence of jumps for most of the droplet lifetime until complete evaporation, Figs. 3.1.a, 3.2.a, 3.3.a and 3.4.a. With an electrode immersed (but without voltage applied), the contact radius decreases and jumps of the contact line are associated with "stick-slip" behavior. It is worth noting that the contact line does not remain completely pinned between jumps: there is a slight drift of the base diameter, possibly due to the hydrophilic effect of the electrode that pulls the contact line. The contact angle shows changes that are correlated with the jumps of the contact line in the case of free evaporation. In order to allow a comparison with the base fluid, the evaporative behavior of the contact line for deionized water has been included for both EW and free evaporation, Fig. 3. A monotonic receding of the contact line, similar to the behavior observed for nanofluids under EW conditions, is reported due to no particles or irregularities on the surface pin the contact line.

Deposits obtained after the evaporation of a nanofluid droplet under EW conditions look more homogeneous, and no rings ("coffee ring stains") are present. TiO_2 nanoparticles present in the bulk of the droplet are attracted uniformly by the positive electrode/dielectric substrate, during evaporation. This suggests a net negative surface charge on these nanoparticles when suspended in deionized water. On the other hand, when no voltage is applied, concentric rings associated with stick-slip behavior are observed [9]. Bigger stains are evident for larger concentrations.

Fig. 4 show the droplet profile with an electrode immersed, for both EW and no EW conditions at four different drying stages: $t = 0$, $t = 1/4t_{evap}$, $t = 2/4t_{evap}$, and $t = 3/4t_{evap}$, where t_{evap} is total evaporation time. Droplet profiles, base line, and theoretical Circle Fitting Fit to the droplet profile were extracted using DSA100 software.

From Fig. 4, it can be observed that the profile at the top of the droplet is altered by the presence of the wire/electrode modifying the typical spherical cap profile induced by surface tension forces. Clear evidence of the affinity of water for the copper wire is presented (low wetting angle).

To support both qualitative results presented, i.e., evaporative behavior and deposits obtained after the complete dry out, and the simple calculations for the nanoparticle electrophoretic speed proposed in the Discussion, an μ_{ep} analysis of the different TiO_2–water nanofluid concentrations with the ZetaPALS Analyzer was carried out. Both μ_{ep} and ξ of the dispersions used during the experimental part were obtained and included in Table 2. ξ is defined as the "net electrokinetic charge" of the particles suspended in a liquid phase at the outer region of the diffusive layer or slipping plane, which is a balance between the surface charge of the particle and the counter-ions present within the electric double layer (EDL) [51,52].

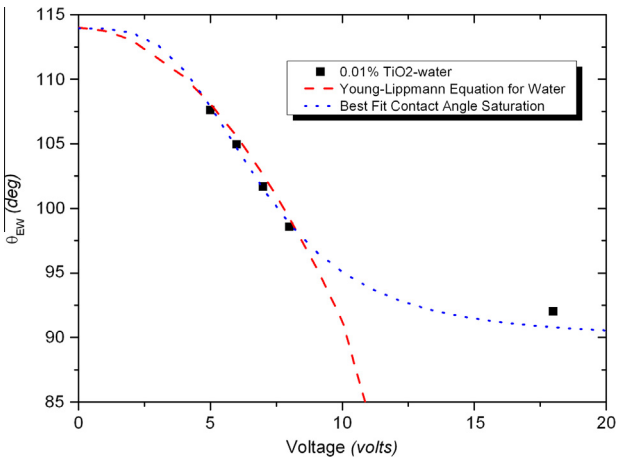

Fig. 2. Experimental EW contact angle, θ_{EW} (°) (squares), versus Voltage, V (V), for 0.01% TiO_2–water nanofluid on $CYTOP_{22}$. Modified Young–Lippmann theory [30] (dashed line) and qualitative θ_{EW} saturation behavior following a best Fit (dotted line) are included.

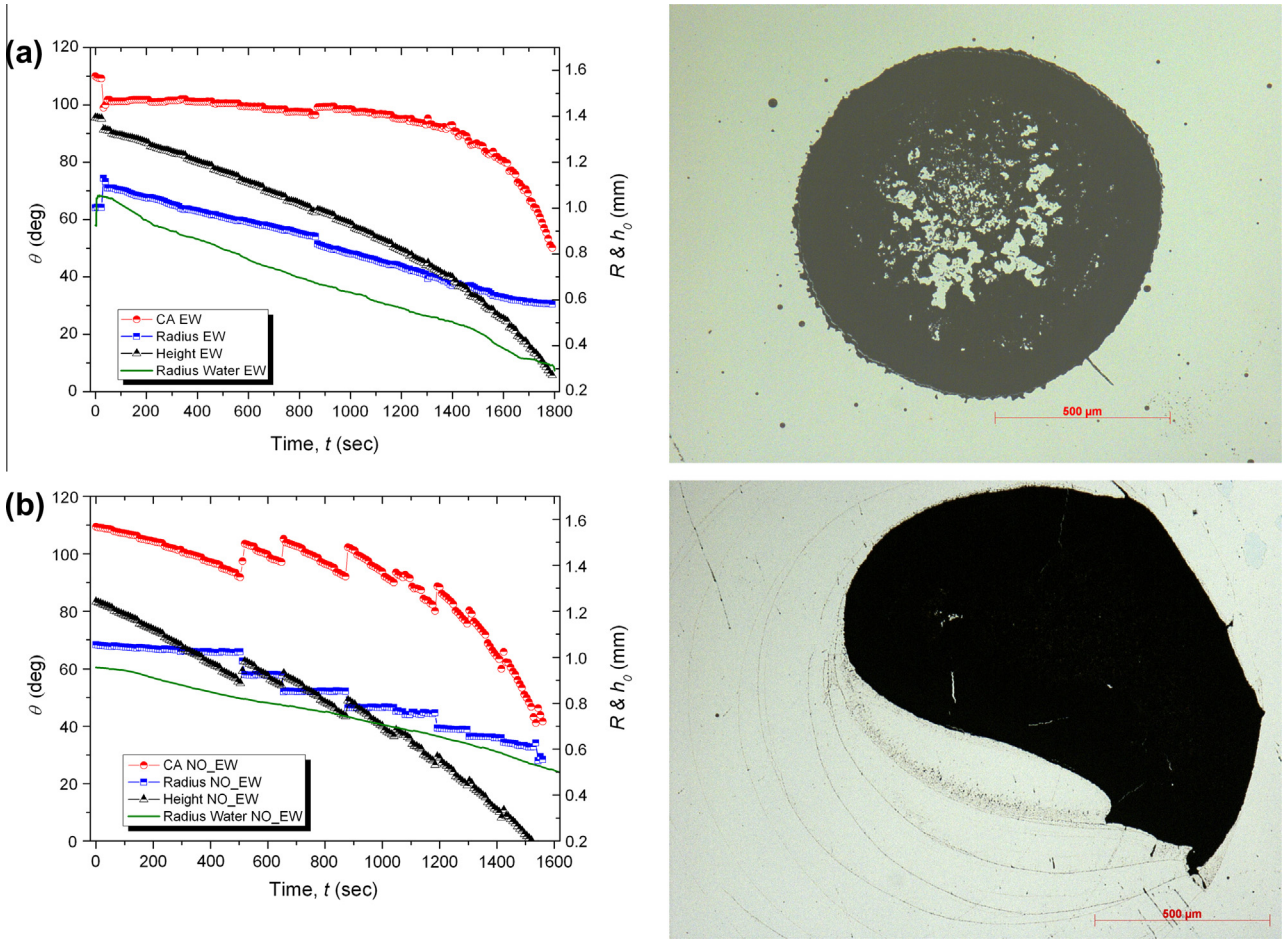

Fig. 3.1. (left) Evolution of the contact radius, R (mm) (squares), contact angle, θ (°) (circles), and height of the droplet, h_0 (mm) (up-triangles), with time, t (s); (a) under electrowetting conditions and (b) under free evaporation of 0.1% TiO_2–water nanofluid. Deionized water contact radius, R (mm) (straight line), versus time, t (s) is included for each case. (right) Corresponding images of the deposits are presented (a) under electrowetting conditions and (b) under free evaporation.

4. Analysis and discussion

The complete evaporation of 3 μl droplets was considered, both under electrowetting and non-electrowetting conditions with an electrode immerse in the droplet. By leaving the electrode in place even for non-EW conditions, similar geometry and conditions of the free liquid surface are ensured. Typically, TiO_2–water nanofluids exhibit "stick-slip" behavior during evaporation, where the contact line remains pinned before the jump ensues, Fig. 3.1.b [9,12]. On the other hand, when DC voltage is applied to a droplet, the principal mechanism by which nanoparticles sediment faster is called electrophoresis. EP was proposed long ago for controlling the deposition of colloidal particles and will lead us to the particle sedimentation velocity [53,54].

We shall attempt to explain the nanoparticle deposit occurring in a relatively even manner, in the case of an applied electric potential. A comparison between the timescales of the two main motions of the nanoparticles within water droplets, namely electrophoretic and advective, is made, i.e., electrokinetic effects are compared to capillary effects due to evaporation, as represented in Fig. 5.

4.1. Advective speed

Initially, we consider the advective speed with which liquid, and therefore nanoparticles, is brought to the triple line under conditions of marked evaporation and pinning [55]. Deegan et al. derived the equation:

$$\rho\frac{\partial h}{\partial t} = -\rho\frac{1}{r}\frac{\partial}{\partial r}(rhv_{adv}) - J_s(r,t)\sqrt{1+(\partial h/\partial r)^2} \tag{2}$$

explaining local change in droplet height, $h(r)$, (at radius r), of an axisymmetric droplet, and depending on time, t The terms ρ, v_{adv} and J are, respectively, liquid density, average radial advective liquid speed, and evaporative mass flux. We are principally interested in what occurs toward the droplet center, where $J_s \approx J_0$, J_0 being evaporative flux from an essentially flat meniscus (diffusion controlled) equal to 1.7×10^{-5} kg/m^{2}s as obtained by additional experiments on free evaporation of water, and $\partial h/\partial r \approx 0$. The height of the droplet (at the center), h_0, decreases approximately linearly, see Fig. 3.1.a, $\partial h_0/\partial t \approx -K$, leading to a simplification of Eq. (2):

$$v_{adv}(r) \approx \frac{r}{2h}\left(K - \frac{J_0}{\rho}\right) \tag{3}$$

Eq. (3) will not describe with any precision what happens at $r = 0$ since flow here will be necessarily vertical, but it allows us to estimate the average advective speed in the vicinity. It has the essential feature predicted by Deegan et al., i.e., $v_{adv} \sim 1/h$, although their description was limited to the contact line region [55]. The actual speed will also depend on height within the liquid, its maximum probably being near mid-height, with decrease both toward the liquid/air and liquid/solid interfaces (less evaporative

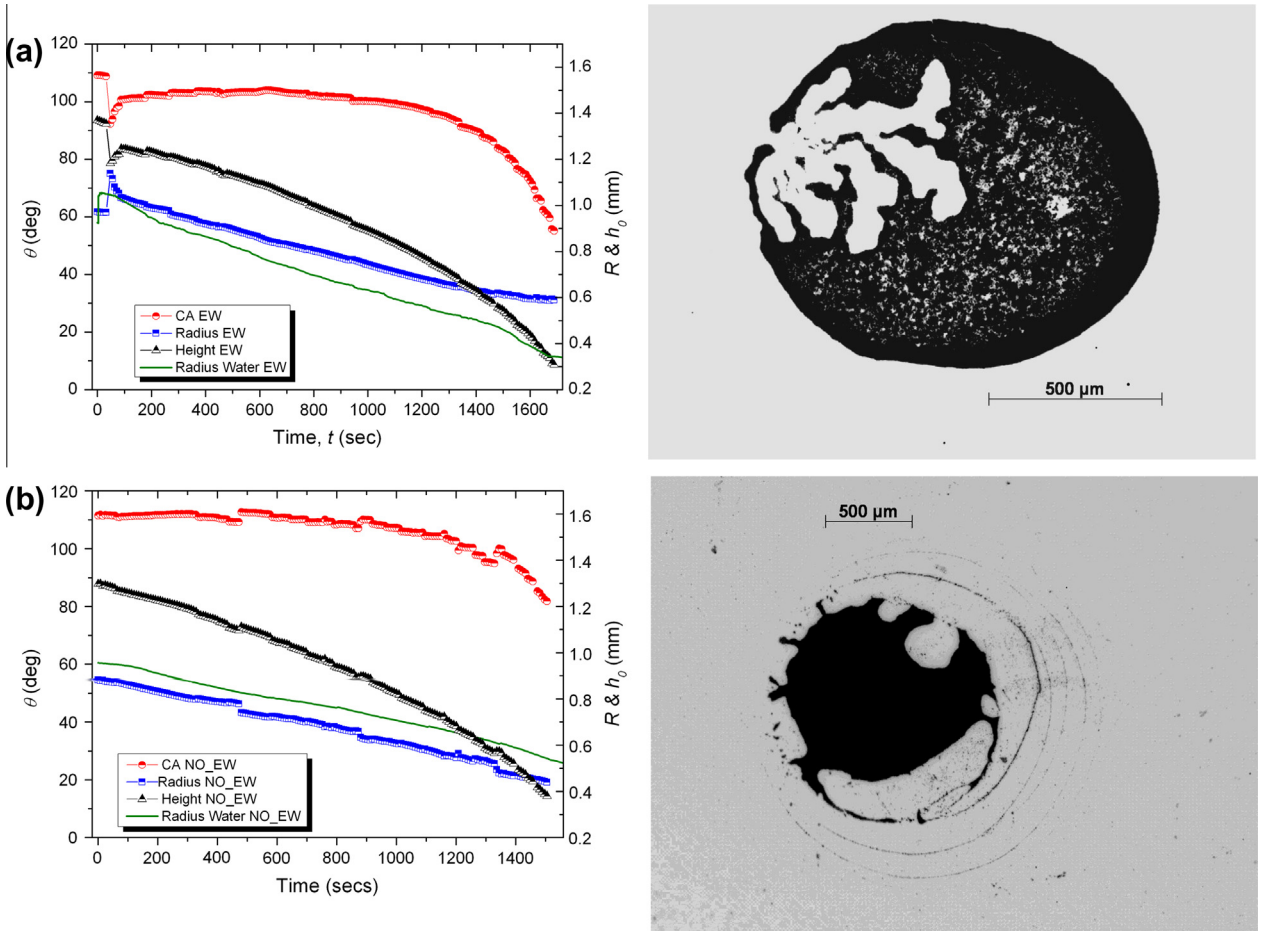

Fig. 3.2. As for Fig. 3.1, but for 0.05% TiO_2–water nanofluid.

activity and greater liquid/solid drag). The "active" distance from the solid for particles deposition would seem to be $\varepsilon \approx 100$ nm [11], and we take ε to be our characteristic distance. We assume that average advective speed in this region is $\sim v_{adv}$. From Fig. 3.1.a, the values of R, droplet contact radius, K, and h, $(h(r) = (R - r)\tan\theta)$, at the beginning of the evaporation process are extracted and substituted in Eq. (3). Then, in the immediate proximity of the contact line $(r \approx R)$, $h \sim (1 - r) \cdot \tan(100^\circ)$mm, $K \sim 6 \times 10^{-4}$ mm/s, a maximum advective velocity of 3 μm/s is obtained. This value is in agreement with the radial particle velocity reported by Marin et al. ~ 3.5 μm/s at the "rush hour" stage and at the vicinity of the contact line [56]. It is worth mentioning that even with the highest advective velocities, which occur toward the end of the droplet lifetime, the electrophoretic timescale will still be shorter than the advective timescale, as will be demonstrated in this section.

Thus far, most of the mathematical models for droplet evaporation are described for a pinned contact line [55,57,58], not "stick-slip" evolution. In order to be able to use this model for our purposes, we attempt to quantify and compare the magnitude of the advective speed to that of the receding contact line. From Fig. 3, the contact line velocity is calculated as: $v_{CL} = \partial R/\partial t \approx 0.3$ μm/s, so a ratio of the two speeds can be obtained, i.e., $v_{adv}/v_{CL} = 3/0.3 \sim 10$. This means that the advective velocity is about one order of magnitude greater than the movement of the contact line, and hence, the displacement of the contact line can be considered as quasi-stationary compared to the advective velocity.

4.2. Electrophoretic speed

Let us now consider any vertical contribution of liquid speed, v_{ep}, absent in normal circumstances (or at least negligible), but potentially important with EW. The electric field within the droplet, E, is not known with any precision, but is given approximately by $E = -\partial V/\partial y \approx V/h_o$, where V is the applied voltage, y is the vertical distance, and h_0 is the droplet height. The nanoparticles used in this study possess intrinsic negative charge, q, when suspended in deionized water as both pictures of the deposits on the positive substrate and additional experiments of the ζ support, Fig. 3 and Table 2, respectively. Then, under an applied electric field, E, nanoparticles will migrate toward the electrode with opposite charge, the dielectric substrate, precipitating by electrophoresis. Analyzing the forces involved when E is applied, a vertical force toward the solid will act on a nanoparticle, $F \downarrow = qE$. This will be balanced by a Stokes-type viscous force, $F \uparrow = 6\pi\eta a v_{ep}$, where η is liquid viscosity and a is (equivalent) particle radius, leading to a drift speed toward the solid surface, v_{ep}, of:

$$v_{ep} \approx \frac{qV}{6\pi h\eta a} \tag{4}$$

Typically, for an isolated spherical particle, ζ can be written as [59,60]:

$$\zeta = \frac{q}{4\pi\varepsilon_r\varepsilon_0 a} - \frac{q}{4\pi\varepsilon_r\varepsilon_0\left(a + \frac{1}{k}\right)} \rightarrow \zeta = \frac{q}{4\pi\varepsilon_r\varepsilon_0 a(ka + 1)} \tag{5}$$

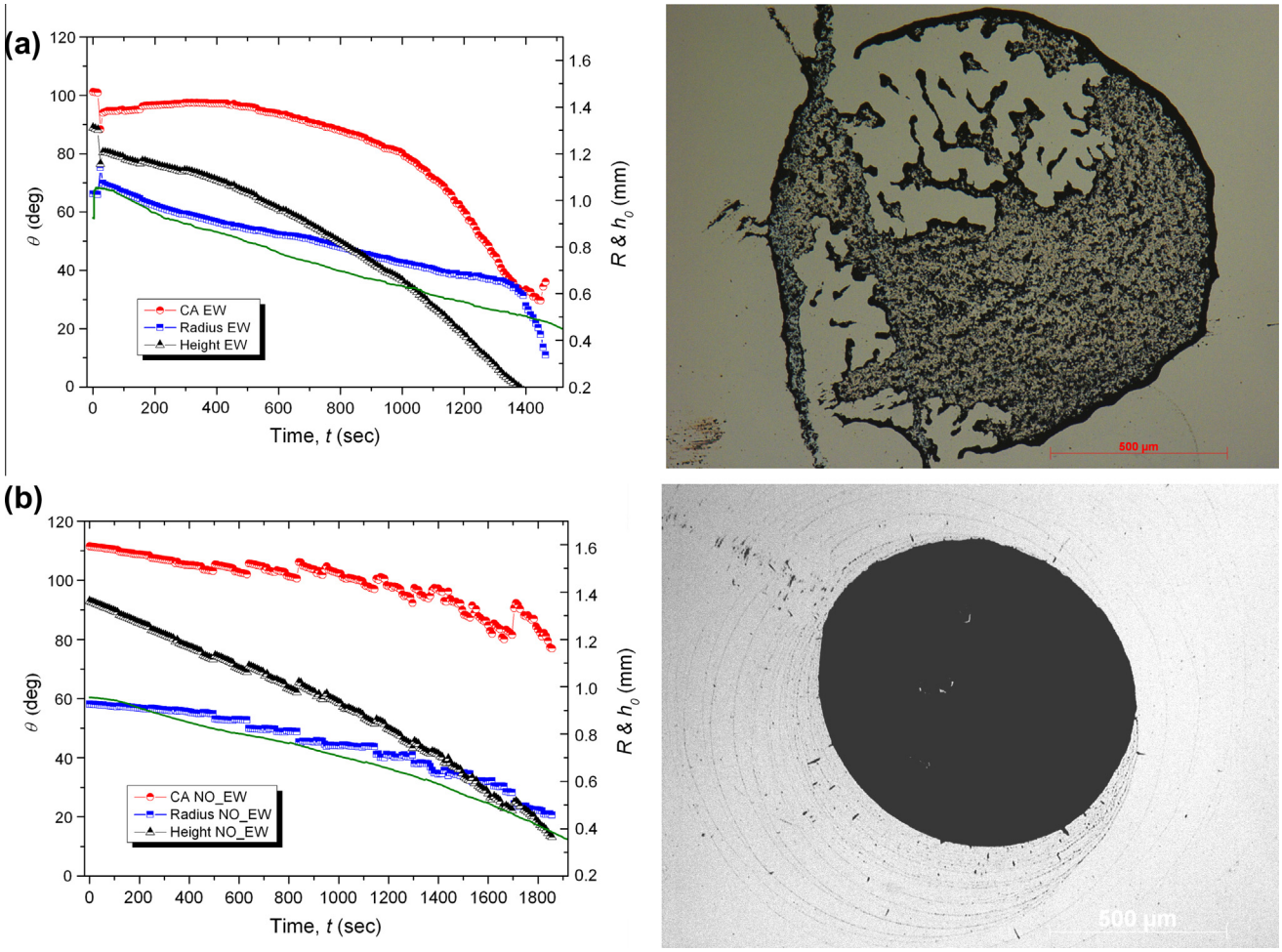

Fig. 3.3. As for Fig. 3.1, but for 0.025% TiO_2–water nanofluid.

Considering *ka* smaller than unity, the effective charge of the particle, *q*, becomes:

$$q = 4\pi a \varepsilon_r \varepsilon_0 \zeta \tag{6}$$

where ε_r and ε_0 are the permittivity of the fluid and in vacuum, respectively. Combining Eq. (4) and Eq. (6), the Hückel equation (Eq. (7)), valid for particle size in the order of nanometers, can be derived and electrophoretic velocity calculated as [50,61]:

$$v_{ep} = \frac{2}{3}\frac{\varepsilon_r \varepsilon_0}{\eta}\zeta\frac{V}{h} \tag{7}$$

An approximation of the EP speed of the nanoparticles within the bulk of the droplet, using Eq. (7) and reasonable values of ζ taken from the literature, is proposed. Substituting the following values: $\zeta = -20$ mV [62,63], $\varepsilon_{H_2O} = 80$, $\varepsilon_0 = 8.85 \times 10^{-12}$ F/m, $\eta_{H_2O} = 1$ cp, $V = 18$ *V* and $h = 0.0014$ m, an EP velocity of approximately 100 μm/s is obtained. This speed is at least one order of magnitude greater than the advective motion of the particles toward the contact line reported by other authors for microliter droplets, that is, ca. 10 μm/s [48,56]. It is worth noting that the electrophoresis experiments carried out by Lee et al. using TiO_2-deionized water are in agreement with the electrophoretic speed calculated using the Hückel equation [42].

To support the electrophoretic velocity calculated using Eq. (7) and values from the literature ($v_{ep} = 100$ μm/s), additional measurements of the electrophoretic mobilities, μ_{ep}, of the nanofluids studied were carried out, results of which are included in Table 2. In electrophoresis, v_{ep} is proportional to the μ_{ep}, and Eq. (7) can be written as follows:

$$v_{ep} = \mu_{ep} \cdot E = \mu_{ep} \cdot V/h \tag{8}$$

Then, for $\mu_{ep} = 1.6$ μm/s/V/cm from Table 2, under 18 V applied and with a distance between electrodes $h = 0.0014$ m $= 0.14$ cm, an v_{ep} ca. 200 μm/s is obtained. This value is of the same order of magnitude as the v_{ep} calculated using values from the literature, and again, it is at least of one order of magnitude greater than internal particle velocities reported due to evaporation [48,56].

4.3. Comparison

As a first approximation, the ratio, $\bar{R} = t_{adv}/t_{ep}$, shows the relative importance of the timescales for the nanoparticles to migrate toward the solid substrate before being swept along to the triple line:

$$\bar{R} = \frac{t_{adv}}{t_{ep}} \approx \frac{v_{ep}}{v_{adv}}\frac{d_{adv}}{d_{ep}} \approx \frac{v_{ep}}{v_{adv}}\frac{1}{1.4} \approx \frac{qV}{4.2\pi\eta a r\dot{h}} \approx \frac{4}{4.2}\frac{\varepsilon_r\varepsilon_0\zeta V}{\eta r\dot{h}} \approx \frac{\varepsilon_r\varepsilon_0}{\eta r\dot{h}}\zeta V \tag{9}$$

When $\bar{R}$ is large, the advective timescale, the time that a particle takes to migrate from the center of the droplet toward the triple line, is greater than the time that the particle takes to reach the charged substrate due to electrophoretic effects. This latter means that the vertical or electrophoretic particle speed, v_{ep}, is greater

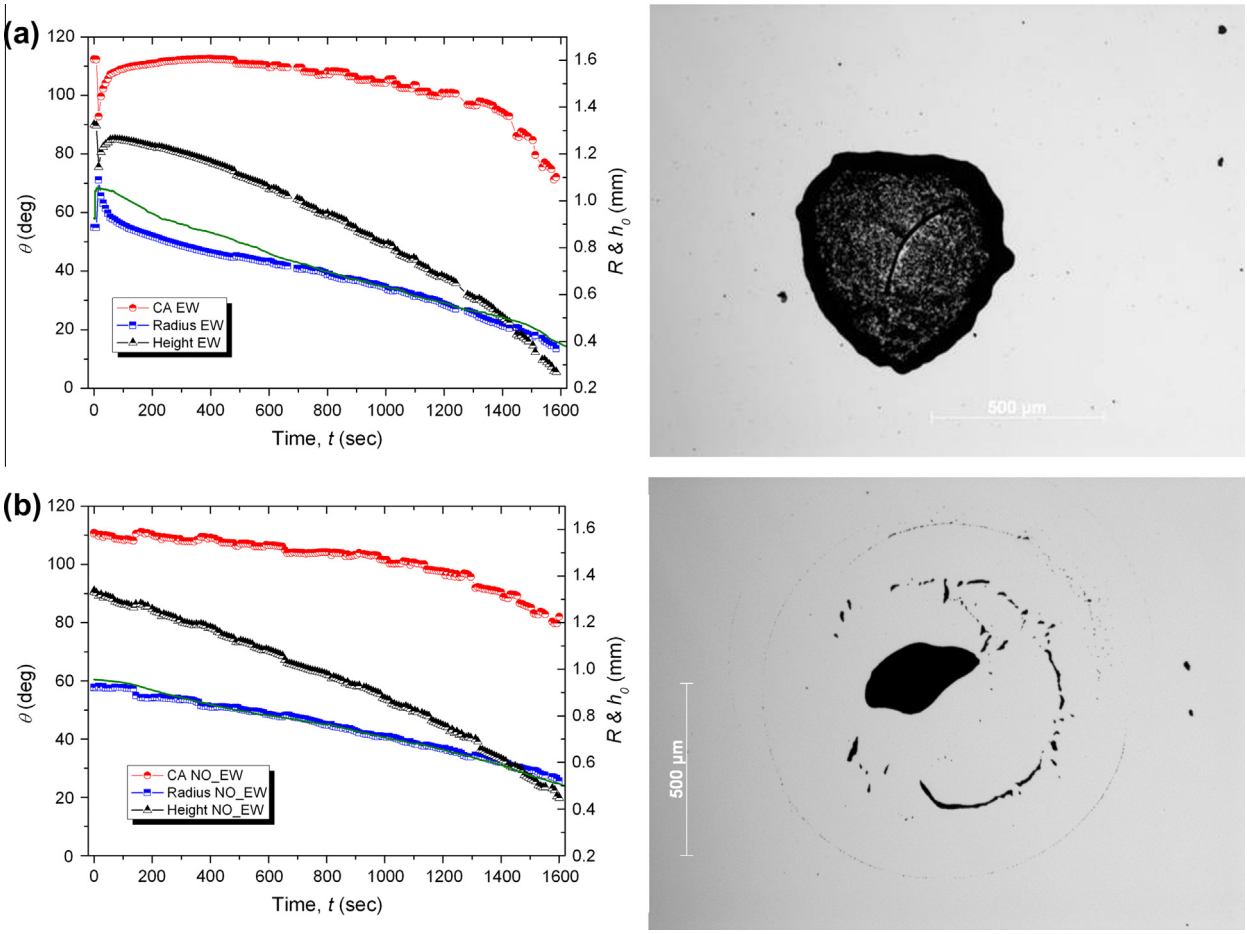

Fig. 3.4. As for Fig. 3.1, but for 0.01% TiO_2–water nanofluid.

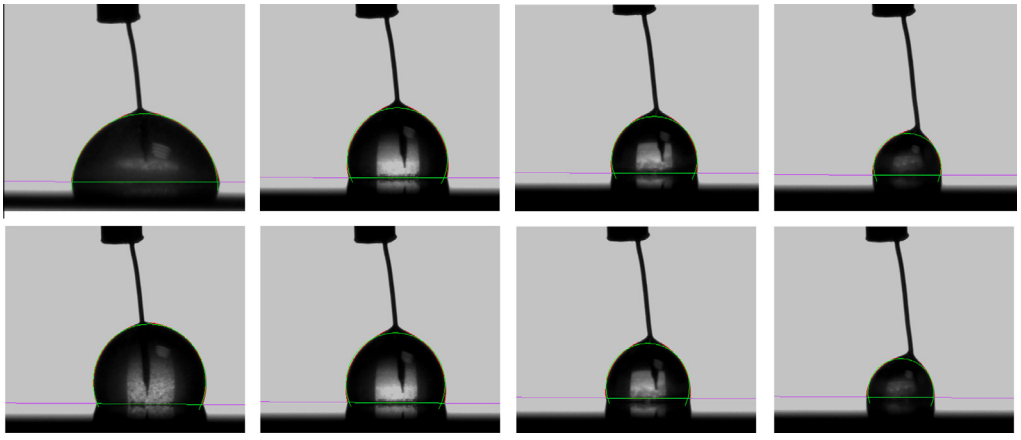

Fig. 4. Droplet profile with an electrode immerse into a 0.05% TiO_2–water nanofluid droplet under (top) applied voltage conditions and (down) no EW. Base line and Circle Fitting Fit are included for $t = 0$, $t = 1/4t_{evap}$, $t = 2/4t_{evap}$ and $t = 3/4t_{evap}$.

than the advective one; therefore, nanoparticles will tend to precipitate onto the solid surface rather than be swept to the triple line, thus leading to a more homogenous final deposit after droplet evaporation. If particles with high surface charge are dispersed in a non-viscous liquid and under a strong electric field, electrophoretic speed will be dominant over advective speed, and particles will move preferentially toward the substrate instead of the contact line.

If we use reasonable values in Eq. (9), i.e., for a 3 μl water droplet $\bar{R} \approx \frac{\varepsilon_r \varepsilon_0}{\eta r \bar{h}} \zeta V \sim 7 \cdot 10^{-4} \frac{\zeta}{\bar{h}} V$ and for $\zeta = -20$ mV and $V = 18$ V,

Table 2
Electrophoretic mobility, μ_{ep} ((μm/s)/(V/cm)), and zeta-potential, ξ (mV), for 0.01%, 0.05%, and 0.1% of TiO_2 nanoparticle concentration by weight in deionized water.

Concentration (%)	Electrophoretic mobility ((μm/s)/(V/cm))	Zeta-potential (mV)
0.01	−2.20 ± 0.07	−43.7 ± 1.6
0.05	−1.65 ± 0.11	−39.0 ± 2.5
0.1	−1.60 ± 0.15	−37.7 ± 3.6

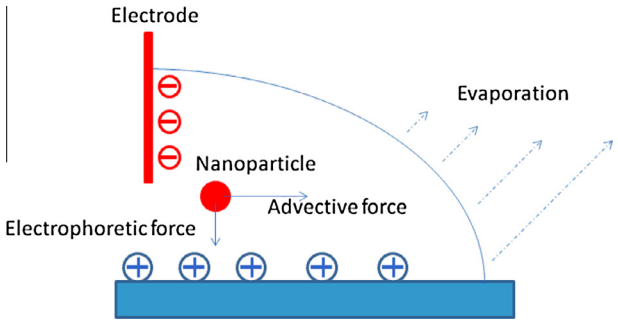

Fig. 5. Electrophoretic and advective motions of a nanoparticle in an evaporating droplet subject to EW.

Table 3
Electrophoretic, v_{ep}, advective, v_{adv} and contact line, v_{CL}, speeds (μm/s), particle migration distance and characteristic time, t_c (s).

	Electrophoretic effect	Advective effect	Contact line motion
Speed (μm/s)	~100.0	~10.0	~0.3
Migration distance ($m \times 10^{-3}$)	1.4	1.0	0.6
Characteristic time (s)	10	100	2000

unless K, the change in droplet shape, is close to 10^{-4} m/s ~ 0.1 mm/s, the electrophoretic motion will be preferential to the advective one. The above calculation is very rudimentary. Not only is the theory simplified, but also various parameters are not well-characterized. Nevertheless, this semi-quantitative analysis gives a plausible explanation of the more homogenous distribution of nanoparticles observed in the zone occupied by the droplets following evaporation under EW conditions, as compared to the well-known accumulation found at the triple line under standard conditions of evaporation.

Numerically comparing the different speeds of displacement of the contact line, the maximum advective speed calculated using Eq. (3), and the electrophoretic speed of the particles obtained from Eq. (7) or Eq. (8), there is an order of magnitude of difference between them, i.e., electrophoretic motion is quicker than advective as it is shown below in Table 3. Charged particles migrate toward an electrode with opposite charge. The sedimentation phenomenon (electrophoresis) competes with motion of nanoparticles toward the contact line (to replenish the liquid evaporated). The fact that the particles are attracted to the substrate and do not accumulate at the contact line hinders particle buildup at the contact line, thus preventing "stick-slip" motion, at least to some extent.

It is demonstrated that the characteristic time for the different phenomena that take place during complete evaporation of a nanofluid droplet under EW conditions differs by at least one order of magnitude. Electrophoretic motion is predominant over advective one; therefore, particles tend to migrate to the substrate with greater speeds than they do toward the contact line; therefore, fewer nanoparticles are expected to reach the triple line, and suppression of "stick-slip" behavior is observed. This allows for a smoother receding of the contact line without pinning. The slow motion of the contact line, compared to the advective speed, agrees with the quasi-steady state assumed during evaporation.

It is well known that the "stick" of the contact line can be due even to irregularities on the surface, so for high concentrations of nanoparticles (0.1%), the suppression of "stick-slip" behavior might not be complete. Some jumps of the contact line were indeed noticed. Hence, the nanoparticle concentrations tested were not high enough for nanoparticles to organize themselves at the edge of the contact line, thus acting as a barrier and impeding contact line recession in the presence of the wire in the EW case.

Regarding the deposits found after complete evaporation, coffee ring deposits are observed following free evaporation with a wire immersed in the droplet and without an applied voltage. In this case, there is a motion of fluid and nanoparticles from the bulk of the droplet toward the contact line to replenish the evaporated fluid. Nanoparticles accumulate at the contact line inducing pinning as the fluid evaporates until the droplet reaches a state of sufficient free energy for a jump of the contact line to occur. At this point, some nanoparticles are left adhering to the substrate leading to the so-called coffee ring stains [7]. Due to the presence of the wire, pinning of the contact line does not occur at constant contact radius. In this case, the contact radius decreases slowly with evaporation before the jump.

On the other hand, evaporation under EW conditions leads to a more homogeneous pattern rather than rings. There is a suppression of the coffee ring stain as shown by our experimental results and also these of other authors [46]. EW hinders accumulation of solutes at the contact line since precipitation seems preferentially. Therefore, potentially, a mechanism to control nanofluid deposit could be achieved using the EW technique. Further work will involve study of complete evaporation under EW for different nanofluids, cells, or bacteria and the effect of EW on nanoparticle structuring [48,64].

During the research carried out and motivated by suppression of the coffee ring stain, another completely different mechanism is proposed for the manipulation and control of nanoparticle deposition with simultaneous EW and evaporation conditions. It has been clearly demonstrated that EP effect drives the particles toward the substrate with greater velocities than the motion of the particles toward the contact line.

5. Additional considerations

For the sake of completeness, it be of interest to consider the possibility in which the oxide nanoparticles present in the bulk of the droplet would move following dielectrophoresis (DEP), since the electric field present inside the droplet is non-uniform [65]. The non-homogeneity of the electric field exerts a gradient of pressure due to the differences between the dielectric properties of the oxide particles and the medium creating an induced dipole, thus DEP motion [66]. Using the experimental data gathered during this experimental research, the DEP speed calculated under our experimental conditions showed smaller values than the advective motion of particles toward the contact line, in the order of few nanometers per second. Therefore, from the homogeneous nanoparticle deposits shown in Fig. 3 and from the electrophoretic analysis carried out and included as Supplementary data, EP is proposed as the more probable main means of transport of nanoparticles in suspension, compared with DEP transport.

6. Conclusions

For the first time, to the authors' knowledge, electrophoresis of TiO_2–water nanofluids has been demonstrated within a droplet subjected to an electric field under DC conditions. The preferential motion of TiO_2 nanoparticles toward the substrate due to electrophoretic forces, instead of to the triple line by advection, has been demonstrated, and the different timescales have been compared. Speeds one order of magnitude greater were found for the electrophoretic effect when compared to the transfer of mass toward the contact line by advection and following evaporation. Electrophoresis (EP) of droplets is proposed as a potential technique to suppress "stick-slip" behavior of contact line and contact angle, where a

monotonic receding of the contact line is reported during almost the entire evaporation. More attractive and homogenous deposits are reported for DC EW experiments due to the EP effect suppressing the coffee ring stain. Therefore, it is proposed as a technique to control nanofluid deposits without altering the dynamics of the contact line during the complete evaporation. Experiments could be extended to cells, bacteria or proteins due to the similar surface charge present in these with respect to dispersed TiO_2 nanoparticles in deionized water. The negative surface charge of TiO_2 nanoparticles, when dispersed in deionized water, has been demonstrated using an inexpensive EW setup and simple evaporation.

Acknowledgments

The authors would like to thank Celine Pastol (Université de Poitiers) for her help during part of this experimental research and Yifan Li from the Scottish Microelectronic Centre (SMC) for the fabrication of the substrates. We would like to acknowledge the help received by Dr. Bryne T. Ngwenya and Mr Derek Jardine on the measurements of the electrophoretic mobilities. Also, we thank the financial support received by the EPSRC.

Appendix A. Supplementary material

Supplementary data associated with this article can be found, in the online version, at http://dx.doi.org/10.1016/j.jcis.2013.05.079.

References

[1] F. Mugele, J.-C. Baret, J. Phys.: Condens. Matter 17 (2005) R705.
[2] T. Leichle, L. Tanguy, L. Nicu, Appl. Phys. Lett. 91 (2007) 224102.
[3] N. Verplanck, Y. Coffinier, V. Thomy, R. Boukherroub, Nanoscale Res. Lett. 2 (2007) 577.
[4] V.W. Kaufui, L. Omar De, Adv. Mech. Eng. (2010) 11.
[5] K. Sefiane, J. Skilling, J. MacGillivray, Adv. Colloid Interface Sci. 138 (2008) 101.
[6] X. Wang, X. Xu, S.U.S. Choi, J. Thermophys. Heat Transfer 13 (1999) 474.
[7] R.D. Deegan, O. Bakajin, T.F. Dupont, G. Huber, S.R. Nagel, T.A. Witten, Nature 389 (1997) 827.
[8] S. Kinge, M. Crego-Calama, D.N. Reinhoudt, Chemphyschem.: Eur. J. Chem. Phys. Phys. Chem. 9 (2008) 20.
[9] J.R. Moffat, K. Sefiane, M.E.R. Shanahan, J. Phys. Chem. B 113 (2009) 8860.
[10] R. Bhardwaj, X. Fang, P. Somasundaran, D. Attinger, Langmuir 26 (2010) 7833.
[11] A. Askounis, D. Orejon, V. Koutsos, K. Sefiane, M.E.R. Shanahan, Soft Matter (2011).
[12] D. Orejon, K. Sefiane, M.E.R. Shanahan, Langmuir 27 (2011) 12834.
[13] F. Mugele, Soft Matter 5 (2009) 3377.
[14] B. Berge, J. Peseux, Eur. Phys. J. E 3 (2000) 159.
[15] C. Quilliet, B. Berge, Curr. Opin. Colloid Interface Sci. 6 (2001) 34.
[16] R.A. Hayes, B.J. Feenstra, Nature 425 (2003) 383.
[17] B.H.W. Hendriks, S. Kuiper, M.A.J. As, C.A. Renders, T.W. Tukker, Opt. Rev. 12 (2005) 255.
[18] J.-L. Lin, G.-B. Lee, Y.-H. Chang, K.-Y. Lien, Langmuir 22 (2005) 484.
[19] H. Kang, J. Kim, In Micro Electro Mechanical Systems, in: 19th IEEE International Conference on 2006, MEMS 2006 Istanbul, 2006, p. 742.
[20] R. Olivier, B. Jean, C. Philippe, B. Mathias, P. Marc, J. Micromech. Microeng. 17 (2007) 2217.
[21] R. Shamai, D. Andelman, B. Berge, R. Hayes, Soft Matter 4 (2008) 38.
[22] T. Krupenkin, J.A. Taylor, Nat. Commun. 2 (2011) 448.
[23] G. Lippmann, Relations Entre Les Phénomènes Électriques et Capillaires, Gauthier-Villars, 1875.
[24] T. Young, Philos. Trans. R. Soc. Lond. 95 (1805) 65.
[25] H.J.J. Verheijen, M.W.J. Prins, Langmuir 15 (1999) 6616.
[26] A. Quinn, R. Sedev, J. Ralston, J. Phys. Chem. B 109 (2005) 6268.
[27] J. Restolho, J.L. Mata, B. Saramago, J. Phys. Chem. C 113 (2009) 9321.
[28] S.H. Ko, H. Lee, K.H. Kang, Langmuir 1094 (2008) 24.
[29] J.S. Kuo, P. Spicar-Mihalic, I. Rodriguez, D.T. Chiu, Langmuir 19 (2002) 250.
[30] Y. Li, W. Parkes, L.I. Haworth, A. Ross, J. Stevenson, A.J. Walton, J. Microelectromech. Syst. 17 (2008) 1481.
[31] R. Malk, Y. Fouillet, L. Davoust, Sensors Actuat. B: Chem. 154 (2011) 191.
[32] P. García-Sánchez, A. Ramos, F. Mugele, Phys. Rev. E 81 (2010) 015303.
[33] F. Mugele, A. Staicu, R. Bakker, D. van den Ende, Lab Chip 2011 (2011) 11.
[34] J.-K. Lee, Environ. Eng. Res. 3 (1998) 97.
[35] P.F. Lee, M. Misran, W.A.T.W. Abdullah, in: N. Osman, W. Abas, A. Wahab, H.-N. Ting (Eds.), 5th Kuala Lumpur International Conference on Biomedical Engineering 2011, vol. 35, Springer, Berlin, Heidelberg, 2011, p. 60.
[36] M.J.G. Janssen, The Titanium Dioxide: Electrolyte Solution Interface, 1984.
[37] F.F. Reuss, Notice sur un nouvel effet de l'électricité galvanique, 1809.
[38] J. Bandy, Q. Zhang, C. Guozhong, Mater. Sci. Applications 2 (2011) 1427.
[39] W.M. Hwang, C.Y. Lee, Bull. Korean Chem. Soc. (2003).
[40] A.H. Jayatissa, Proc. SPIE 5592, Nanofabrication: Technologies, Devices and Applications (2005), 400.
[41] N. Surugau, P.L. Urban, J. Sep. Sci. 2009 (1889) 32.
[42] P.F. Lee, Ph.D. thesis, Jabatan Kimia, Fakulti Sains, University Malaya, Kuala Lumpur, Malaysia, 2009.
[43] H. Moon, S.K. Cho, R.L. Garrell, C.-J. Kim, J. Appl. Phys. 92 (2002) 4080.
[44] R.K. Dash, T. Borca-Tasciuc, A. Purkayastha, G. Ramanath, Nanotechnology 18 (2007) 475711.
[45] M.E.R. Shanahan, Langmuir 1041 (1995) 11.
[46] H.B. Eral, D.M. Augustine, M.H.G. Duits, F. Mugele, Soft Matter 7 (2011) 4954.
[47] H.B. Eral, D. van den Ende, F. Mugele, Physics World 2012, April 2012.
[48] D. Mampallil, H.B. Eral, D. van den Ende, F. Mugele, Soft Matter 8 (2012) 10614.
[49] E. Seyrat, R.A. Hayes, J. Appl. Phys. 90 (2001) 1383.
[50] BIC Instruction Manual for ZetaPALS, Zeta Potential Analyzer, New York, 1999.
[51] H.J. Butt, K. Graf, M. Kappl, Physics and Chemistry of Interfaces, Wiley, 2006.
[52] J. Lyklema, Fundamentals of Interface and Colloid Science, Academic Press, 1991.
[53] R.C. Hayward, D.A. Saville, I.A. Aksay, Nature (2000) 404.
[54] O.D. Velev, K.H. Bhatt, Soft Matter 2 (2006) 738.
[55] R.D. Deegan, O. Bakajin, T.F. Dupont, G. Huber, S.R. Nagel, T.A. Witten, Phys. Rev. E 62 (2000) 756.
[56] Á.G. Marín, H. Gelderblom, D. Lohse, J.H. Snoeijer, Phys. Rev. Lett. 107 (2011) 085502.
[57] H. Hu, R.G. Larson, J. Phys. Chem. B 106 (2002) 1334.
[58] Y.O. Popov, Phys. Rev. E 71 (2005) 036313.
[59] D.J. Shaw, Introduction to Colloid and Surface Chemistry, fourth ed., Butterworth-Heinemann/Elsevier Science, Oxford, 1992.
[60] J.H. Lyklema, Fundamentals of Interface and Colloid Science: Solid–Liquid Interfaces, Academic Press, 1995.
[61] E. Hückel, Phys. Z. (1924) 25.
[62] S. Hussain, S. Smulders, V. De Vooght, B. Ectors, S. Boland, F. Marano, K. Van Landuyt, B. Nemery, P. Hoet, J. Vanoirbeek, Particle Fibre Toxicol. 9 (2012) 15.
[63] C.P. Tso, C.M. Zhung, Y.H. Shih, Y.M. Tseng, S.C. Wu, R.A. Doong, Water Sci. Technol.: J. Int. Assoc. Water Pollut. Res. 61 (2010) 127.
[64] A. Askounis, K. Sefiane, V. Koutsos, M.E.R. Shanahan, Phys. Rev. E 87 (2013) 012301.
[65] T.B. Jones, Electromechanics of Particles, Cambridge University Press, 1995.
[66] L.D. Landau, E.M. Lifshitz, L.P. Pitaevskiĭ, Electrodynamics of Continuous Media, Pergamon, 1984.